Environmental Earth Sciences (2018) 77:500
https://doi.org/10.1007/s12665-018-7675-0

ORIGINAL ARTICLE

Soil erosion and chemical weathering in a region with typical karst topography

Kai Xiong[1] · Chuan Yin[2] · Hongbing Ji[1,3,4]

Received: 27 February 2017 / Accepted: 26 June 2018
© Springer-Verlag GmbH Germany, part of Springer Nature 2018

Abstract

Soil erosion is a global environmental issue that can lead to the loss of nutrient-rich topsoil and even soil desertification, which is more severe in vulnerable and sensitive karst areas. Currently, it is imperative to explore the soil erosion mechanism and the weathering process to help prevent soil degradation in the karst area. In this study, we estimated the soil erosion rate of a representative karst slope in Shilin area of China by ^{137}Cs tracer method. We also analyzed the changes of soil total organic carbon (TOC), total nitrogen (TN), and total phosphorus (TP) along the soil profiles. The results show that there is mild to moderate intensity erosion in this area, and erosion rates in different locations of slope are in the following order: hilltop > hillside > bottom. The ^{137}Cs content has a certain correlation with TOC, TN and TP content in the soil profile, which indicates they may have similar loss pathways. Furthermore, the chemical index of alteration (CIA), Na/K value and their relation with soil erosion are analyzed and reveal that the studied area is seriously affected by physical erosion and chemical weathering under a hot and humid environment area.

Keywords Erosion rate · ^{137}Cs tracer method · Chemical index of alteration · Southwest China · Karst slopes

Introduction

Karstic geological and ecological systems, which provide approximately 20–25% of the world's drinking water (Parise et al. 2015), are important parts of the earth's surface system and their changes will have an impact on other regions and even the entire Earth system. However, currently the soil erosion in karst areas has seriously threatened the local agriculture and livelihoods of local residents (Bai 2011), especially when the soil erosion is not considered in the past planning of urban and industrial development (Bathrellos et al. 2012, 2017; Papadopoulou-Vrynioti et al. 2013). In fact, quantifying the soil erosion rate and chemical weathering intensity in karst areas can provide data support for future industrial upgrading and the conservation of water and soil (Buttafuoco et al. 2012; Rozos et al. 2013; Perović et al. 2013). In the past several years, despite many works studied the soil erosion in karst areas (Kheir et al. 2008; Bai 2011; Feng et al. 2016), relatively few works focused on both soil erosion and chemical weathering in these areas (Millot et al. 2002; Gabet 2007; Krishnaswamo and Gyana 2012). Exploring the relationship between physical erosion rates and chemical weathering can help us to understand the formation and long-term evolution of weathering profiles in karst areas. Generally, physical erosion accelerates chemical weathering by weakening bedrock and providing a fresh mineral surface for chemical weathering, while chemical weathering accelerates physical erosion by dissolving primary minerals (Ferrier and Kirchner 2008; Clift et al. 2014). Accordingly, it is widely accepted that physical erosion enhances chemical weathering in geology (Schoonejans

Electronic supplementary material The online version of this article (https://doi.org/10.1007/s12665-018-7675-0) contains supplementary material, which is available to authorized users.

✉ Hongbing Ji
ji.hongbing@hotmail.com

1 Beijing Municipal Key Laboratory of Resource Environment and GIS, College of Resource Environment and Tourism, Capital Normal University, Beijing 100048, China

2 School of Geomatics and Urban Information, Beijing University of Civil Engineering and Architecture, Beijing 100044, China

3 School of Energy and Environmental Engineering, University of Science and Technology Beijing, Beijing 100083, China

4 State Key Laboratory of Environmental Geochemistry, Institute of Geochemistry, Chinese Academy of Sciences, Guiyang 550002, China

Published online: 02 July 2018

et al. 2016) and vice versa (Blanckenburg 2005; Braun et al. 2005). For example, in landslide-dominated landscapes, the theoretical model by Gabet (2007) shows the rate of chemical weathering do increase with erosion rates and is proportional to the erosion rate raised to the ~0.6 power. By cosmogenic nuclide methods, Kirchner et al. (2006) measured the rates of physical erosion and chemical weathering in granitic terrain. They found the "Weathering Intensity Factor" (WIF), ratio of the chemical weathering rate to the physical erosion rate, is temperature dependent, which is attributed to the biologically mediated weathering. In fact, chemical weathering begins when organisms (microbes, moss, etc.) emerge from the hard rock surface, and the weathering reactions can be further efficiently catalyzed by vegetation and microbes. The substances generated by the biological metabolism process, such as oxygen and organic acids, would further accelerate the process of chemical weathering and affect the soil erosion rate (Kirchner et al. 2006). In addition, the precipitation can lead to both soil erosion and chemical weathering (Chetelat et al. 2008).

From the geochemical perspective, the physical erosion and weathering of the surface drives the material circulation. Chemical weathering is mainly limited by the supply of fresh minerals by erosion especially in areas with steep slopes (Kirchner et al. 2006). The more intense the physical erosion is, the more severe the chemical weathering is (Anderson et al. 2007). However, Gabet and Mudd (2009) pointed out that the relationship of weathering intensity and erosion rates is not simply a linear one. As the erosion rates increase, the potential increases in weathering rate due to the exposure of fresh minerals are offset by the decrease in the total volume of minerals exposed. Accordingly, at high erosion rates, the weathering rate increases slowly and sometimes even decline (Gabet and Mudd 2009). Many previous researches were focused on the primary and moderate weathering in the temperate zone (Chen et al. 2008; Shao et al. 2012), whereas studies on soils under the extreme weathering conditions were few. The elements (e.g. Ti, Zr) that were considered stable in temperate study areas are now proved to occur obvious movement under strong chemical weathering (Kurtz et al. 2001). In fact, the migration of elements in strong chemical weathering areas is quite different from that in moderate areas (Xu and Liu 2007). For the Yunnan Karst area, which is strongly influenced by karst environmental heterogeneity, the geochemical composition of karst surface must be affected by the weathering of rock and soil (Tang et al. 2010). However, the physical erosion and chemical weathering of watersheds vary between localities due to different regional hydrodynamic conditions, topography, ecology, seasonal climate, and other factors (Yang et al. 2014). This increases the difficulty of exploring the mechanism of soil erosion in the karst area. Therefore, it is of great importance to study the soil erosion and weathering in the carbonate area and understand the trends of soil and water loss in this region.

The ^{137}Cs tracer method can be used to accurately compute the average soil erosion rate over long periods. It has, therefore, been widely used in many countries and regions (Takahashi et al. 2015; Li et al. 2016; Molla and Sisheber 2017). Verheijen (2009) first suggested that there is a close relationship between the redistribution of ^{137}Cs in the soil and the migration of the eroded soil for areas with small soil erosion. This provides the fundamental theory for tracing soil erosion via ^{137}Cs. Gaspar et al. (2013) used the fallout radionuclides ^{137}Cs, $^{210}Pb_{ex}$, and ^{7}Be as tracers of sediment mobilization and redistribution, which makes it possible to estimate soil redistribution rates within both undisturbed and cultivated landscapes over a range of timescales. An elegant theoretical soil erosion model set up by Zhang et al. (1990) can be used to obtain soil erosion rate from the distribution of ^{137}Cs along the soil profile. Yang et al. (2014) investigated the specific activity and distribution of ^{137}Cs in Karst hillslopes of the central Guizhou plateau and then discussed the main influencing factors. The study found that the specific activity of ^{137}Cs in Guizhou was higher than that in western Yunnan. Due to the severe rock desertification of Shilin Karst slopes in Yunnan, uneven soil distribution, and widely exposed bedrock, ^{137}Cs would enter soils in the bedrock crevice with rainfall, which leads to the distribution of ^{137}Cs in the karst slopes different from other areas.

The objectives of this study are: (1) to reveal the mechanism of soil erosion in the karst areas; (2) to show the migration of soil nutrients along the karst slope under long-term soil erosion, and (3) to clarify the relationship between the soil erosion rate and the chemical weathering intensity in the karst areas. Our results show that both physical erosion and chemical weathering play an important role in the soil erosion process in the karst areas.

Materials and methods

Study area

The sampling site is in the Karst area of Shilin Yi Autonomous County (24°48'N, 103°19'E) which is 78 km away from Kunming, China. It is characterized by peak cluster depression, limestone, and sandy soil. It experiences 2250 h of average annual sunshine, and the annual average temperature is approximately 16.3 °C. It is also an area influenced by the intersection of monsoons (Indian Ocean southwest monsoon and Pacific southeast monsoon). The frost-free period is 240 days annually. The annual average rainfall is between 800 and 850 mm, with the May–October rainy season precipitation accounting for 86% of annual precipitation. It is marked by a subtropical low-latitude mountain

plateau monsoon climate. The elevation is in the range of 1600–1900 m, with higher terrain in the southwest and lower terrain in the northeast. From east to west, the Karst mountain road that leads to the southern basin is gently inclined and transitions into Karst slope. The upper part of the slope is mostly steep with inclination of approximately 30°, the lower part of the slope is gentler at substantially less than 10°, and the middle slope is within the range of 15°–20°.

Soil sampling and data analysis

Samples were collected in April 2015. The sampling points are located in surrounding natural secondary forest low mountain slopes in Shilin. The various cracks or karren karsts of stone pillar is one of the habitats for plants, also the place for vegetation closely related to Shilin area to grow. As for zonal vegetation under present situation, first, the most evident characteristic of stony habitat growing vegetation lies in a small area of semi-humid broad-leaved forest, with diagnostic species as *Cyclobalanopsis glaucoides* schottky, *Castanopsis orthacantha* and *Lithocarpus dealbatus*. Second, shrubby vegetation is relatively stable in this area. Calcium-preferred ferns have the strongest presence, due to their features such as small, shade preferred, calcium preferred, and their preference to grow on epiphytic rocks. The representative species are *Sophora davidii, Pistacia weinmannifolia, Diospyros mollifolia*, etc. The topographic map of the sampling area is shown in Fig. 1. The topographic profile method is used to collect samples. For each study site, samples are collected from the top of the slope to the foot, and then five typical soil profiles are selected with an interval of 5 m. A total of 73 research samples are collected. For each sample, the soil profile was dug vertically downwards with a shovel and continuously sampled downwards from the top soil at a 3-cm interval, each collecting about 2 kg. The sampling point profile is shown in Fig. 2. The basic information such as elevation data of each sample was also documented. Sampling depth is generally at the 35–40 cm layer. When cross-sectional soil deposition occurs, the sampling depth is greater than 40 cm, which may exceed the depth of the soil containing ^{137}Cs (Li et al. 2009).

Soil samples were air-dried. Weeds and pebbles were removed, and then samples were subjected to sieving (sieve opening size 2.0 mm). Samples were then dried to constant weight at 110 °C. After these samples cooled, 380 g were extracted using a balance with accuracy of 0.001 g and then be put in the plastic containers of the same specifications. These subsamples were placed in plastic containers and kept the surface flat. ^{137}Cs specific activity analysis uses an energy-dispersive spectrometer (eds). We used a 16,384 multi-channel analyzer of the S-100 series made by Canberra in USA. It exhibits high stability. Main technical indicators of the spectrometer: the energy resolution of γ spectrometer measurement system is 2.25 keV at 60Co1.33 MeV, peak/compton ratio higher than 60:1, relative detection efficiency at 62%, measurement time for each sample is 28800s (real time), measurement error controlled under 95%, data test deviation smaller than 5%. The specific activity of ^{137}Cs is obtained from the γ-ray spectrum area at 661.6 keV. The activity is then multiplied by the soil volume and thickness, which produces area-specific activity with the units of Bq/m^2. Total amount of ^{137}Cs (Bq/m^2) is the sum of ^{137}Cs area-specific activity in all soil layers from the surface to the depth where it is completely undetected. The method uses the following formula:

$$\mathrm{CPI} = \sum_{i=1}^{n} 10^3 \times C_i \times B_i \times D_i . \quad (1)$$

CPI (^{137}Cs Point Inventory) represents the total amount of ^{137}Cs in sample, i indicates the layer number, n represents the layer numbers of sample, C_i stands for specific radioactivity of ^{137}Cs in the ith sample layer (Bq/g), B_i indicates soil bulk density of the ith sample layer (g/cm^3), and D_i for thickness of the ith sample layer (cm).

We prepared the samples before the measurement and completed the experimental procedure as follows. First, we picked out all plant roots from surface soil, then left them for natural drying, crushed the clods and quartered them as in common practice. For each time of reduction, we mixed the test samples evenly. The final sample was around 200 g. We spread the sample on the foil and put it into a dryer at a temperature below 50 °C for 48 h. The dried sample would then be handled by an automatic ball grinder to 200 mesh, and preserved in a self-sealing bag or sealed bottle for later testing. Before grinding each sample, the mortar of ball grinder shall be scrubbed and cleaned with water repeatedly, dried with dryer, wiped with ethanol and then blow-dried.

Constant element determination is conducted by Philips PW2402 model X-ray fluorescence spectrometer. The measurement of TN and TP in soil samples is taken by persulfate digestion method (Mitchell et al. 1996). TOC is the amount of carbon found in an organic compound, and is an important material basis for soil, and is also one of the important indexes for measuring soil quality. A TOC analyzer (Shimadzu, TOC-LCSH) and a solid sampler (SSM-5000-a) were used to analyze TOC in soil samples. 200 mg dried soil samples is transferred to ceramic boat after through a 200-mesh sieve. The test samples together with purified air are put into the high-temperature combustion tube to measure the amount of total carbon (TC) and low-temperature reaction tube to measure the amount of inorganic carbon (IC). TOC is calculated by subtraction of the IC value from the TC value in the sample.

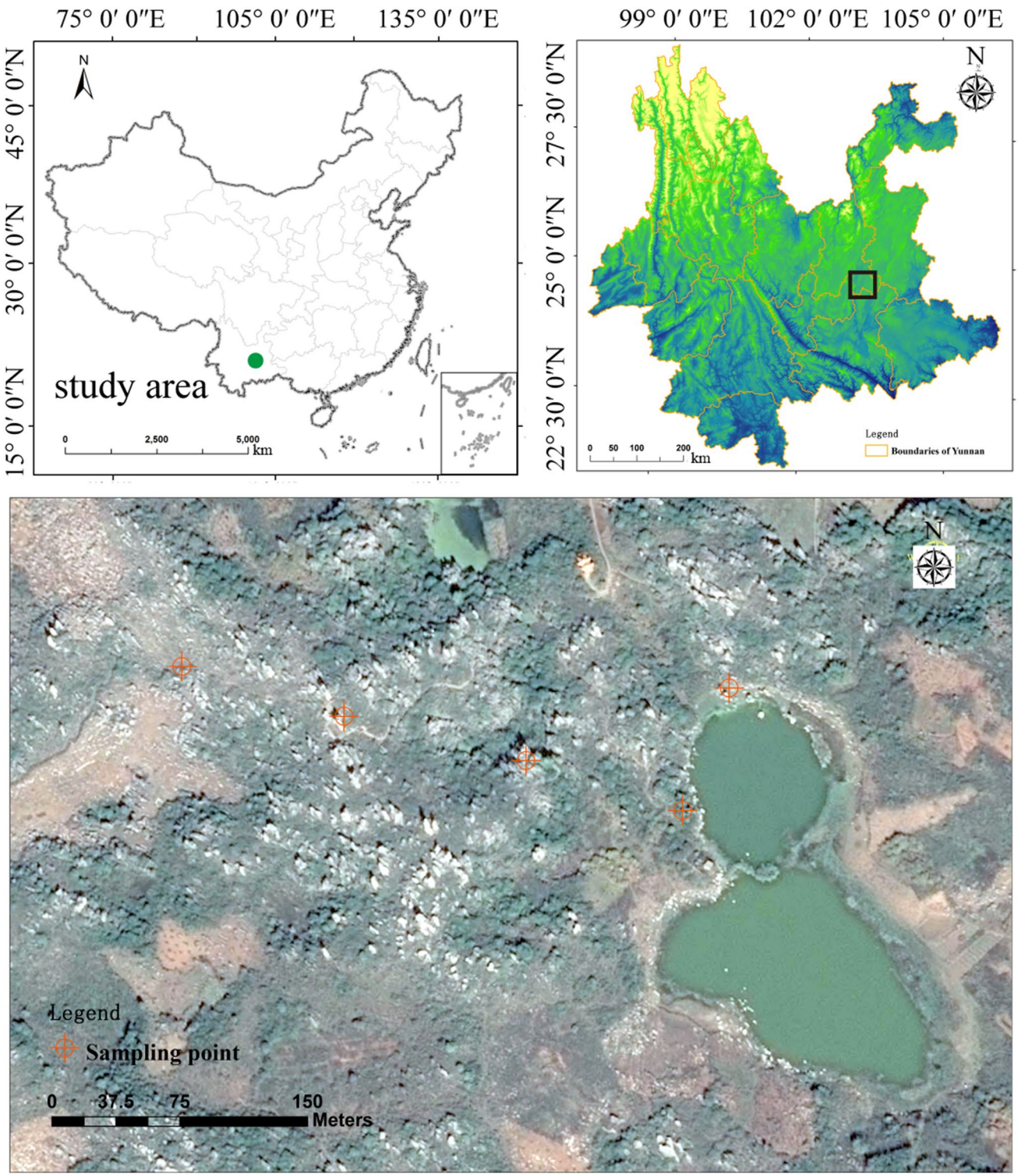

Fig. 1 Simulated landform map of sampling sites

The determination of background value

^{137}Cs background value is the total amount of ^{137}Cs per unit area of ground settlement (Bq/m^2). It is necessary to determine the background value of ^{137}Cs in a research area to apply the tracer method to estimate soil erosion, as this directly affects the accuracy of soil erosion modulus or soil erosion rate. There are two ways to determine the

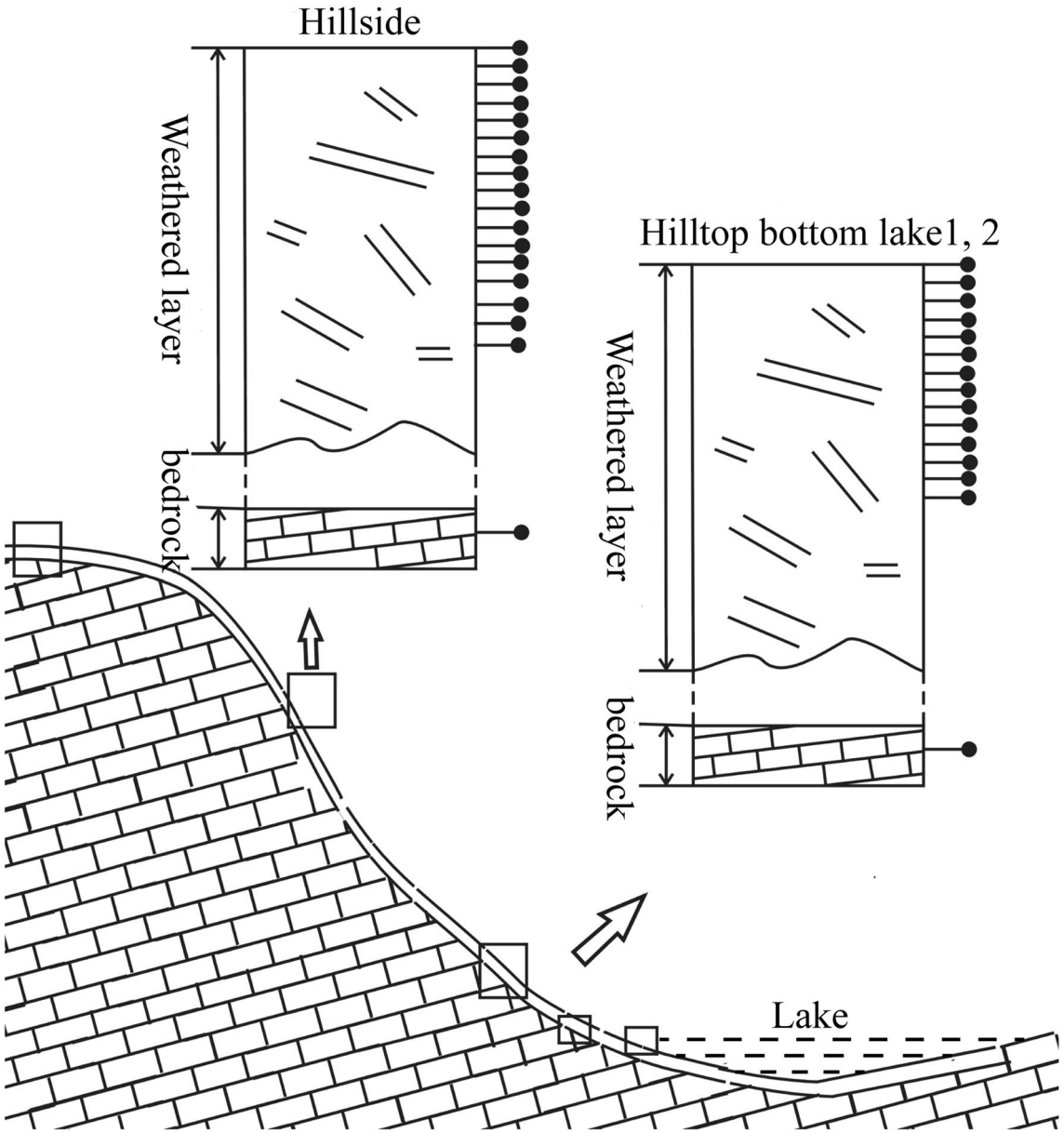

Fig. 2 The profile information of Shilin, China

background value: one is to directly measure ^{137}Cs content in a sample from an undisturbed area with relatively little erosion and deposition; and the other one is to record the background value directly in the same basin. This second method can only be applied if weather conditions and ^{137}Cs spatial distribution are consistent. In general, the selected benchmarks are sites that have experienced relatively little erosion or deposition for more than 50 years. In this research area, it is difficult to find such sampling points. In fact, it will produce a great loss of ^{137}Cs under weak erosion. And in this area the precipitation is concentrated, so the soil is severely lost by hydraulic erosion, and it is even lower than the estimated values. Therefore, it is not suitable as a reference point. Landscape and the pitch of the slope are important factors affecting local soil erosion rate. Owens acquired an estimate of annual settlement of ^{137}Cs from 1954 to 1990 in the northern hemisphere. Based on the geographical coordinates and precipitation, Qi and Zhang obtained the background value of ^{137}Cs in different regions of China by computational simulation, and the background value of Dongchuan area near our study area is 1269 Bq/m^2 (Zhang et al. 2010). According to the global simulation by Walling and Owens (1996), it can be concluded that the ^{137}Cs background value in this

region is 860 Bq/m^2. In contrast, Niu et al. (2014) and others measured the background value of Dianchi lake area in Yunnan as 906 Bq/m^2. Considering that this research area and Dianchi lake area are at the same latitude with 50.66 km of separation and experience almost the same average annual rainfall, we set the ^{137}Cs background value of the research area as 906 Bq/m^2, which has also been adopted and considered as reasonable by other researchers.

Mathematical model for calculation of soil erosion with ^{137}Cs method

The key issue in the application of ^{137}Cs tracer technique to the estimation of soil erosion is the conversion of the change in ^{137}Cs content to soil erosion rate. There are two important components to this method: one is the need to accurately measure the local ^{137}Cs background value, and the other is a reasonable soil erosion model. In this study, we selected to collect soil samples in the slope land which is in long-term lack of human disturbance. In most occasions, ^{137}Cs gathers in the surface layer, and its distribution exponentially decreases with depth in the undisturbed soil. Based on the report of many researchers on the exponential distribution of ^{137}Cs in non-farming soil profiles, Zhang et al. (1990) provides a function for ^{137}Cs profile distribution:

$$A'(x) = A_{\text{ref}}\left(1 - e^{-\lambda x}\right). \tag{2}$$

x represents the soil depth (cm), is the total amount of ^{137}Cs between 0 and x in depth (Bq/m^2), and is the profile exponential of ^{137}Cs depth distribution (cm^{-1}).

For example, assume that the sedimentation of ^{137}Cs occurred in 1963 and its distribution and depth in the soil profile were not influenced by temporal changes. The annual erosion thickness h of the erosion pitting can be calculated by the following equation:

$$h = -\frac{1}{(t-1963)\lambda}\ln\left[\left(1-\frac{x}{100}\right)\right], \tag{3}$$

where h is the erosion rate (cm/a), t is the sampling year, and x is the decreased percentage compared to background value $(A_{\text{ref}}-A)/A_{\text{ref}} \times 100$.

Soil erosion modulus indicates the intensity of soil erosion, showing the intensity of erosion intensity in a certain region per unit time.

The modulus of the soil erosion is calculated as follows:

$$Y = h \times D \times 10000. \tag{4}$$

Y is for soil erosion modulus (t/km^2/a) and D is for soil capacity (Kg/m^3).

If the background value is input into the equation, the ^{137}Cs content in the soil profile is more than the point of background value. This indicates that there is soil deposition.

Chemical Index of Alteration

The change in absolute content of a single element cannot accurately reflect the evolution of chemical weathering intensity as it is influenced by elemental leaching migration and re-deposition. This is why chemical weathering degree is often measured by an element content index or ratio.

The Chemical Index of Alteration (CIA) is widely applied as a geochemical indicator of chemical weathering degree. The CIA value is proportional to the amount of feldspar that transforms into clay minerals by weathering. Hence, the chemical weathering degree of silicate minerals can be quantitatively explained. The stronger weathering of sediment is followed by a higher CIA. The formula for CIA is as follows (Nesbitt et al. 1982):

$$\text{CIA} = [\text{Al}_2\text{O}_3/(\text{Al}_2\text{O}_3 + \text{Na}_2\text{O} + \text{K}_2\text{O} + \text{CaO}^*] \times 100. \tag{5}$$

In the formula, Al_2O_3, CaO, K_2O, and Na_2O are input moles of oxide molecules, CaO* is the molar content of silicate minerals. The combined Ca (Nesbitt et al. 1989) in the carbonate, phosphate, and other minerals is not included. It is clearly observed in the geochemical movement of elements in the surface that CIA reflects the degree of clay minerals weathered by aluminosilicate minerals, especially feldspars (Kautz and Martin 2007). A higher CIA indicates more leaching of Na, K, and Ca in the silicate minerals from parent rocks, as well as a stronger effect of chemical weathering (Nesbitt and Young 1996). During the study, the accurate isolation and purification of silicate minerals from sediments has proven difficult. Therefore, the correction method proposed by McLennan (1993) is applied in this study. The CIA is calculated based on the average composition of Na and Ca in natural silicate minerals and the molar ratio of CaO/Na_2O in the sediment sample. The CaO is replaced by the molar content of Na_2O if the ratio is more than 1. If the ratio is less than 1, the CIA is calculated directly from the molar content of CaO, which is equivalent to m CaO* = m CaO.

Results and discussion

Caesium distribution in soil profile

Five soil profiles were analyzed in this study, and the distribution of ^{137}Cs in these soil profiles is shown in Fig. 3. From the distribution of ^{137}Cs activity in different soil profiles, we can see that the soil erosion rates and deposition rates vary greatly in different locations. Figure 3a shows soil samples collected on the top of slope (hilltop), with a soil sampling depth of 40 cm and an area-specific activity

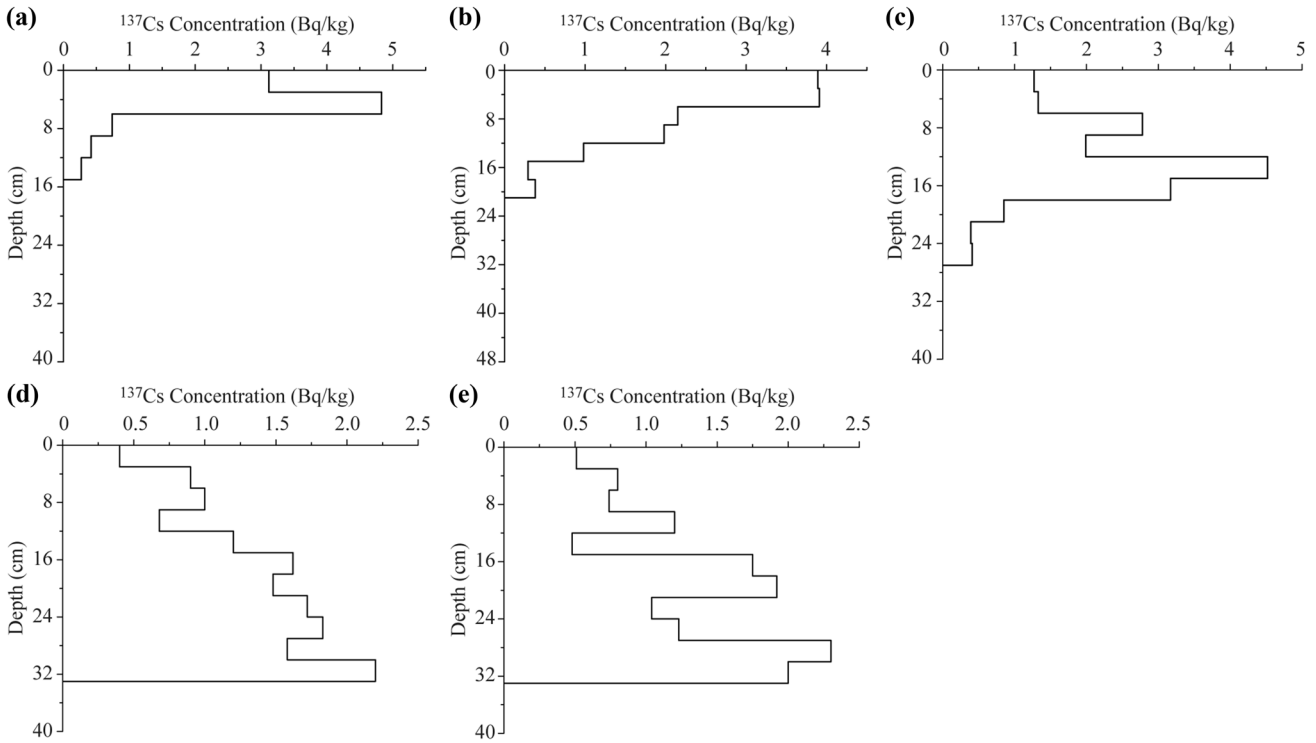

Fig. 3 ^{137}Cs depth distribution features. Sampling depth is 40 cm, a cross-sectional soil deposition occurs, and the sampling depth is greater than 40 cm, more than likely contain soil depth of ^{137}Cs

of 428.5 Bq/m^2. Figure 3b shows soil samples collected in the middle of the slope (hillside), with the sampling depth of 48 cm and an area-specific activity of 645.9 Bq/m^2. Figure 3c shows soil collected on the lower part of the slope (bottom), with the sampling depth of 40 cm and an area-specific activity of 983.7 Bq/m^2. As shown in Fig. 3a, b, the ^{137}Cs content is lower than the background value on the hilltop and hillside, and it is mainly distributed in the soil with the depth of 0–6 cm, similar to previous studies (Pumpanen et al. 2016) that there is a relative enrichment layer of ^{137}Cs in the range of 3–6 cm. Below 3 cm, the ^{137}Cs content decreases exponentially with the increase of soil depth, indicating that the upper soil particles move slowly to the lower layer. There are several reasons for these patterns. First, the distribution is related to the sedimentation history of ^{137}Cs. From the beginning to the completion of sedimentation, ^{137}Cs sedimentation flux is basically a single-peak curve with the highest sedimentation flux in the mid-1960s. Second, ^{137}Cs are mainly adsorbed in the fine particles of the soil with half of them in the soil particles with diameters less than 0.001 m (Henry et al. 2013). The fine soil particles are easy to migrate to the deep soil under the action of gravity and leaching of rainwater, and the fine particles are vulnerable to wind erosion. In Fig. 3a, the peak of ^{137}Cs on the hilltop is not located in the topsoil, which may be related to diffusion and migration of ^{137}Cs with rain. If the sampling sites have been corroded by rain for a long time with strong soil leaching, migration infiltration rate of ^{137}Cs in soil profile will be greater than its own diffusion infiltration rate, and ^{137}Cs concentration in subsurface soil will be higher than that in the topsoil. The distribution depths of ^{137}Cs in different soil profiles are in in the following order: hilltop < hillside < bottom. According to Nearing et al. (2015), the specific activity of ^{137}Cs is affected by many factors, such as climatic conditions, vegetation, topography and so on. The sampling slope is slower with a thicker cover of leaves and branches in Fig. 3b, c. At the bottom of the slope (Fig. 3c), there is a peak of ^{137}Cs under the topsoil (12–15 cm) with a concentration of 4.52 Bq kg^{-1} and the activity of total area is higher than the background value, indicating that there is some sedimentation at the foot of the slope. This may be due to soil erosion on the slopes, as the ^{137}Cs in the topsoil particles migrates down via gravity or rain, wind, and other mild erosion. Figure 3d, e shows soil collected in the washland (lake 1 and lake 2). ^{137}Cs in these profiles is deeply distributed in the soil with a sampling depth of 50 cm. The specific activities of the areas are 1038.8 and 1109.7 Bq/m^2, respectively. These activities are 14.7 and 22.5% higher than the local ^{137}Cs background value of 906 Bq/m^2, which indicates sedimentation occurred at these two sampling points. The ^{137}Cs

content in the washland profile exhibits an exponential increasing trend, although there is some fluctuation along the profile. This is because sedimentation and erosion occur alternately under the influence of water erosion at different flow rates during the formation and evolution of the washland.

Using the soil erosion and sediment models presented above, the soil erosion rates of hilltop, hillside and bottom are 0.216, 0.188 and 0.067 cm/a, respectively. This shows that in the sampled slope, the soil erosion intensity decreases as the elevation decreases. The sediment rates of lake1 and lake2 are − 0.105 and − 0.117 cm/a, respectively, less than the sum of the erosion rates on hilltop and hillside. This suggests that part of the eroded soil is deposited on bottom and washland, and the rest may flow into the river. Overall, the ^{137}Cs concentration varies significantly along the slope. Compared with the background value, the loss is quite large. One possible reason is that rocky desertification is serious in the study area, and ^{137}Cs is not easily adsorbed by bedrock, which leads to the loss of ^{137}Cs with rainfall. The other possible reason is that the migration of ^{137}Cs along the slope is mainly affected by the downward flux of rainwater and the organic matter in the soil. The adsorption or immobilization of ^{137}Cs by organic matter makes it accumulate in the topsoil, whereas rainfall makes it migrate downward.

Due to the shallow and scattered soils with bare rocks in the Shilin area, the soil erosion mechanisms are different at each site. Previous studies have shown that the spatial distribution of ^{137}Cs may be affected to some extent by the underground soil loss (Peng and Wang 2012; Wang et al. 2014). However, in the present study, the specific activity of ^{137}Cs did not show a discontinuous trace distribution in the profile. This phenomenon indicates that soil particles did not run off the ground with the negative surface topography along the rainfall, and the soil formation process in the area is a combination of hilltop erosion and hillside sedimentation. Also, this soil formation process shows the spatial distribution of ^{137}Cs caused by profile erosion and is not affected by underground soil loss. Therefore, when investigating the soil erosion in karst areas by ^{137}Cs tracing method, the surface topography needs to be fully considered.

Soil erosion modulus estimation

According to the Eq. (4), soil erosion modulus of this region can be calculated and the results are shown in Table 1. In the study area, the soil erosion rate and the ^{137}Cs content are closely related to the local slope and topography. Slope is an important factor affecting soil erosion. Generally, the slope is positively related to soil erosion rate, i.e. the amount of ^{137}Cs loss and the erosion modulus increases as the slope increases.

As shown in Table 1, from the hilltop to the bottom the ^{137}Cs content in the soil is increasing and the amount of soil loss is decreasing. The soil erosion rates at different topography are as follows: hilltop > hillside > bottom. And the soil erosion modulus at the hilltop reaches 3345.4 t/km^2/a. This is because the hilltop is steeper and the vegetation coverage is worse than that on the hillside and the bottom. In addition, 80% of the annual precipitation is concentrated in the rainy season, resulting in large surface runoff and flow velocity, and large scouring force on the slope. At the bottom and washland, the soil erosion is relatively light, and even soil sedimentation occurs. On the one hand, it may be due to the smaller slope gradient at the bottom and correspondingly lower water flow velocity, resulting in partial soil sedimentation on the bottom and washland. On the other hand, Kavian et al. (2014) and Lanznaster et al. (2010) have shown that vegetation cover is usually negatively correlated with soil erosion. There are only grass plants on the top of the slope, but there is rich vegetation coverage at the bottom of the slope with dry branches and fallen leaves, weeds, and shrubs which may greatly reduce soil erosion.

According to the soil erosion intensity classification standard issued by the Water and Soil Conservation Monitoring Center Of China's Ministry of Water Resources and the Institute of Remote Sensing of the Chinese Academy of Sciences, mild, moderate, severe erosion, and extreme strength erosion modulus are defined as < 500, 500–2499, 2500–4999, 5000–7999, 8000–15,000, and > 15,000 t/

Table 1 Landscapes, gradient, ^{137}Cs Content and soil erosion modulus of typical longitudinal profile sampling site

Sampling site	Land-use type	Landscapes	Gradient (°)	^{137}Cs content (Bq/m^2)	Soil erosion modulus (t/km^2.a)
a	Natural secondary forest in low mountains and hills	Hilltop	28	428.5	3345.4
b	Natural secondary forest in low mountains and hills	Hillside	17	645.9	1765.2
c	Natural secondary forest in low mountains and hills	Bottom	5.5	983.7	73.5
d	Natural secondary forest in low mountains and hills	Lake 1	0	1038.8	− 857.3
e	Natural secondary forest in low mountains and hills	Lake 2	0	1109.7	− 1321.8

km^2/a, respectively, in low hilly areas of South China. Soil erosion in this area belongs to the mild and moderate erosion.

Change in soil erosion rate and the chemical substance content of soil

The water content, soil capacity, and soil texture are closely related to chemical substance content of soil. Therefore, the change in soil quality caused by soil erosion will affect the chemical content in soil. By investigating the relationship between the soil erosion rate and the change of chemical content in soil, we can predict the change of soil chemical content when we monitor the ^{137}Cs content change. Generally, TN, TP and TOC, which influences the stable structure of soil, are selected as indicators of soil quality, because these substances will affect the local and surrounding ecological environment with the soil erosion. In this study TOC, TN, and TP are measured in soil samples at different slope position. The variation of these chemical elements along the soil profiles is shown in Fig. 4.

TOC change in soil

As shown in Fig. 4, the topsoil has the largest TOC content, and the TOC content declines with the increase in soil depth, which indicates that topsoil is more conducive to the storage of soil TOC (Lenka et al. 2012). Meanwhile, the decrease of TOC content is different at different slope positions. At the hilltop (H1), the TOC content is decreased: from 5.49 to 0.27%, a decrease of 95.08%; at the hillside (H2), from 6.25 to 0.99%, a decrease of 84.16%; at the bottom(B), from 4.57 to 1.18%, a decrease of 74.17%; at the lake 1 (L1), from 4.64 to 1.86%, a decrease of 59.91%; and at the lake 2 (L2), from 4.85 to 1.98%, a decrease of 59.17%. In profiles H1 and H2, the TOC content drops sharply with increasing depth, dropping to 0.30 and 0.99% at 30 cm, respectively, while remaining relatively stable without apparent fluctuation from 35 to 50 cm. The reason for this pattern is the serious soil erosion of the first two profiles. The TOC content in the surface layer is the largest due to the role of vegetation retention. The TOC content decreases rapidly with depth because of the small amount of nutrients that are infiltrated into deeper soil. The TOC content of profile B still presents a downward trend with the increase of depth, but this trend is not obvious as in the first two sample locations. There is slight fluctuation at 20 to 30 cm, but the overall content is relatively stable due to the good vegetation coverage at the foot of the slope foot and the soil sedimentation at this location.

The changes of TOC content in L1 and L2 profiles are small with a range of 23.6–25.1%. TOC here also shows a decreasing trend and then remains stable with the increase of sediment depth, which may be associated with the deep soil moisture. Since both profiles are washlands, high soil moisture can dissolve more TOC into the soil; and some organic carbon from microbial decomposition can also migrate via the water permeability and add to deep soil organic carbon.

To better understand the relationship between soil erosion and soil nutrient content change, correlation analysis was performed between ^{137}Cs activity and soil TOC in the study area. Figure 5 shows that there is an extreme positive correlation between ^{137}Cs content and TOC content in soil, with a correlation coefficient of 0.98. This supports the idea that the change of soil erosion degree has a huge impact on soil TOC content in the study area. As the soil erosion increases, the loss of the TOC content also will increase significantly.

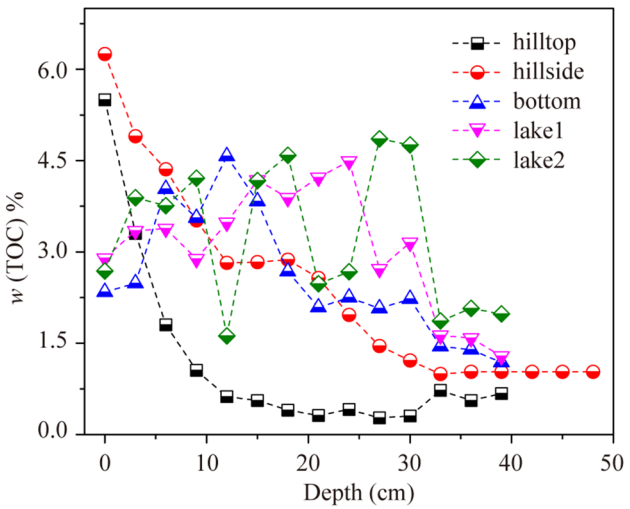

Fig. 4 Characteristics of soil TOC in different portions of the slope

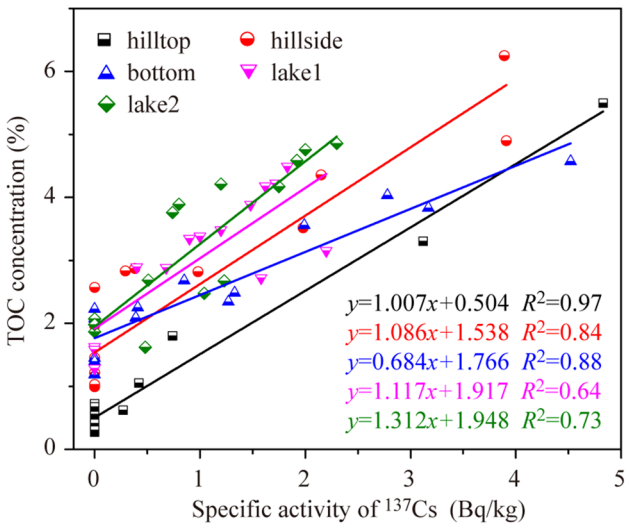

Fig. 5 Relationship between ^{137}Cs and TOC content in secondary forest slopes

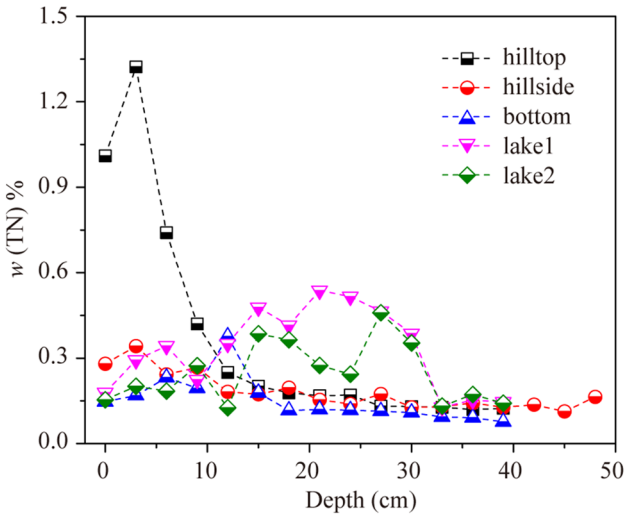

Fig. 6 Characteristics of soil TN in different portions of the slope

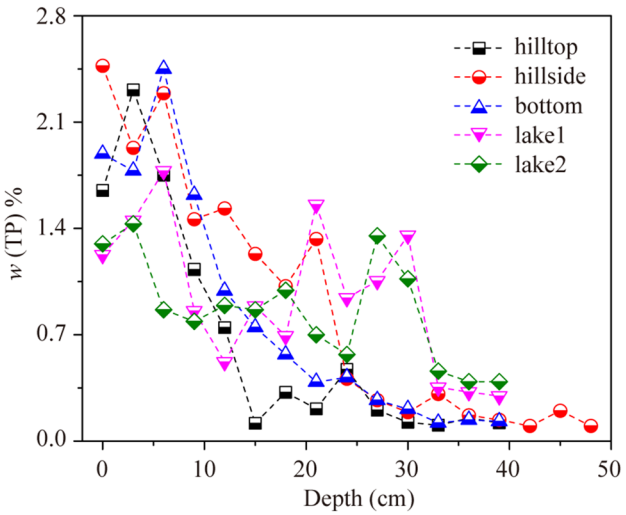

Fig. 7 Characteristics of soil TP in different portions of slope

TN change in soil

As shown in Figs. 4 and 6, the change of TN content in soil is highly consistent with that of TOC along the soil profiles. This phenomenon has been confirmed by many researchers, i.e. the TOC content and TN content in soil have a significant positive correlation (Fu et al. 2010; Gelaw et al. 2014; Tripathi et al. 2014). In this study, the TOC and TN content show an extremely significant positive correlation (Fig. 5), and the correlation coefficient values are $r_1 = 0.96$, $r_2 = 0.89$, $r_3 = 0.88$, $r_4 = 0.86$, and $r_5 = 0.83$, respectively, for profiles H1, H2, B, L1, and L2. At the hilltop and hillside, the TN content in topsoil is generally higher than that in deep soil, where the nitrogen is relatively stable (Fig. 6). This is because the nitrogen in soil mainly comes from the N_2 in the atmosphere, the degradation of some animal and plant residues, and the biological nitrogen fixation of atmospheric nitrogen and precipitation. Therefore, the nitrogen is relatively concentrated in the 0–10 cm soil layer which represents the plant root system distribution area. The superior ability to store TN is also consistent with previous studies (Yang et al. 2013; Zhang et al. 2013). For profiles B, L1 and L2, the TN content does not drop sharply with the depth of the soil, which is due to its low elevation and soil sedimentation. H1 and H2 are washlands, and TN content does not exhibit large differences between layers due to higher soil saturation, stronger aggregation capability, and decomposition of animal feces. To understand the relationship between soil erosion and TN content, correlation analysis was carried out. Results show that there is a significant negative correlation between the soil erosion rate and TN content ($R = 0.95$, $P < 0.01$), and higher soil erosion rates generally result in lower soil TOC and TN content.

TP change in soil

Compared to TOC and TN in soil, the change in TP exhibits a much gentler decline. As a sedimentary mineral, TP has the least material migration in weathered shells (Dai et al. 2015). As shown in Fig. 7, the TP content exhibits irregular fluctuations along the soil profiles. TP content of profile H1 ranges from 0.104 to 2.31 mg/g, with a mean of 0.55 mg/g. TP content of H2 ranges from 0.10 to 2.47 mg/g, with a mean of 0.51 mg/g. TP content of B ranges from 0.12 to 2.45 mg/g, with a mean of 0.49 mg/g. TP content of L1 ranges from 0.29 to 1.77 mg/g, with a mean of 0.56 mg/g. TP content of L2 ranges from 0.39 to 1.43 mg/g, with a mean of 0.54 mg/g, which is consistent with the usual level of TP content in southern acidic soil (according to the second soil census, TP content of soil in South China is generally less than 0.56 mg/g). Phosphorus is a typical sediment cycle element and a sedimentary mineral, which has the smallest migration among the weathering crust. TP exhibits some correlation with ^{137}Cs content ($R = 0.64$, $p < 0.01$), and its loss and transfer should also be concerned. The phosphorus lost via soil erosion may eventually accumulate in the lake and cause eutrophication in the watershed.

The ^{137}Cs migrated along the soil profile are mainly affected by the downward flux of rainwater and the soil organic carbon content (Niu et al. 2014). The adsorption or fixation of organic carbon makes ^{137}Cs enrichment in the topsoil and its downward migration is limited (Ritchie et al. 2007). In this study, ^{137}Cs in all profiles showed a significant positive correlation with soil TOC content, which is consistent with the general law. The distribution characteristics of soil nutrients TN and TP were also investigated, and the results show that the specific activity of ^{137}Cs is consistent and correlated with the distribution of TOC, TN and TP

along the soil profile in the Shilin area, indicating they may have the same loss pathways. In addition, it also shows that the topography has an important influence on soil development, and the soil at the foot of the slope is more likely to accumulate TOC, TN and TP.

Chemical weathering intensity (CIA)

Generally, there is a close relationship between physical erosion and chemical weathering. Erosion can accelerate or slow down weathering, and weathering is the prerequisite of erosion. The rate of soil formation by weathering is also the major theoretical basis to formulate allowance of soil erosion loss. A CIA value between 50 and 65 represents low chemical weathering intensity under cold and dry weather; values between 65 and 85 represent moderate chemical weathering intensity under warm and humid weather; and values between 85 and 100 represent strong chemical weathering intensity under hot and humid weather (Babechuk et al. 2014).

According to the definition of chemical weathering intensity, it can be seen that the chemical weathering intensity of the soil samples in the five soil profiles are relatively high (Fig. 8). The lowest value is 91.2, the highest value is 97.4, and the average value is 95.1. The CIA value indicates that the area undergoes intense chemical weathering under subtropical conditions. The feldspar, plagioclase in particular, is rich in Na. Potassium feldspar, illite, and mica contain K. The weathering resistance of plagioclase is much weaker than potash feldspar; therefore, the Na/K value can be used as an indicator of weathering degree in plagioclase samples and can also be used to indicate the chemical weathering degree of sediments (Bian et al. 2014). The CIA was inversely proportional to the Na/K value in this study. The correlation coefficients (R) were −0.87, −0.91, −0.95, −0.89 and −0.86, respectively, indicating that the Na/K value in these areas can serve as a sound indicator of chemical weathering intensity (Fig. 8). CIA values are highest at the hilltop and hillside, which indicates the chemical weathering is strongest there. Low vegetation coverage, exposed bedrock, and low maturity rate of soil in the two slope positions are the major causes. Note the soil erosion is also very strong at the hilltop and hillside.

The chemical weathering trend is usually represented by a ternary diagram of A–CN–K (Al_2O_3–[CaO*+NaO]–K_2O), which can also reflect the change in the composition of main minerals during chemical weathering. A–CN–K ternary diagram (Al_2O_3–CaO*+NaO–K_2O) can present different stages of chemical weathering clearly as well as changes in some main elements at different stages. Based on the difference of element activity, chemical weathering can be divided into three stages: the initial stage of Na and Ca removal, the middle stage of K elimination, and the late stage of Si elimination. The ternary diagram in Fig. 9 shows that the trends in the five profiles of our study area are basically parallel to A–K boundary, far from K apex, and close to A apex, with a quite long distance to the UCC (upper continental crust). This suggests that the soil has gone through the first two stages and is entering the late stage of Si removal and Fe enrichment. The plagioclase in the profile has been almost completely removed via weathering. The weathering trend is parallel to the A–K boundary, and gradually approaches the A apex. This clearly illustrates a clear trend of K removal

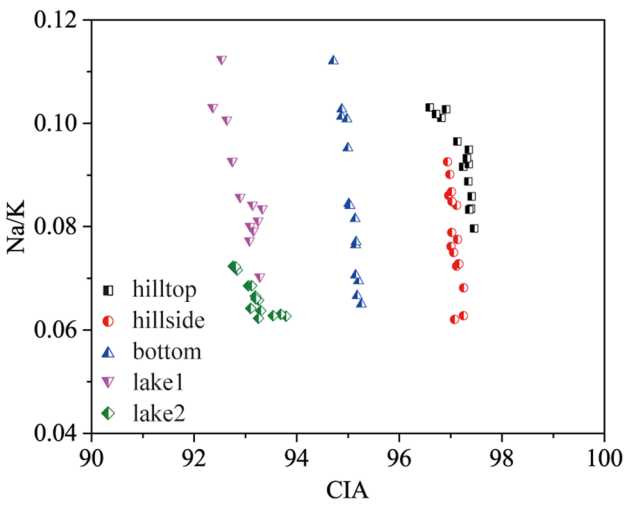

Fig. 8 Scatter graph of CIA vs. Na/K molar ratio in the karst slope of Shilin. Chemical Alteration Index (CIA) is the use of constant elements (silicate oxide) in the Al_2O_3, Na_2O, K_2O, and CaO changes as a measure of the degree of chemical weathering

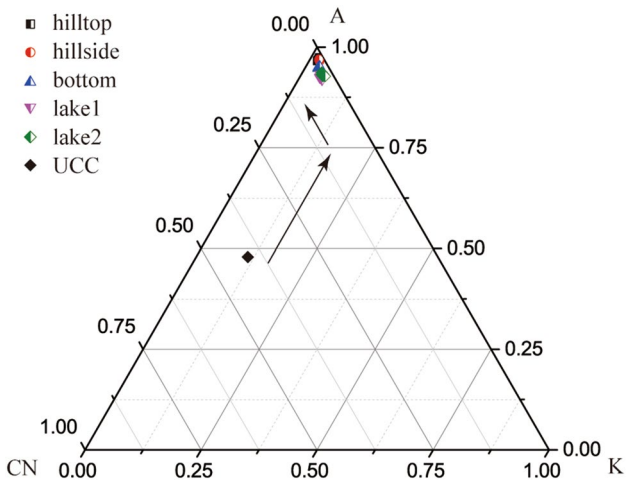

Fig. 9 A–CN–K ternary diagram of the karst slope in Shilin (arrows indicating weathering trend). This can reflect the chemical weathering trends and chemical weathering process of principal components and mineralogy changes where, A, CN, and K, respectively, represent Al_2O_3, CaO + Na_2O (CaO refers to the silicate part of the Ca), and K_2O molecular ratio

and Al enrichment. With increases in climate temperature and humidity, leaching migration leads to decreased content of CaO, Na_2O, and K_2O while Al_2O_3 and Fe_2O_3 is relatively stable. In summary, the soil in the area has undergone relatively intense weathering. The figures of the five profiles are all converging to one point in the diagram, suggesting a similar weathering process.

Chemical weathering occurs and new minerals form when rocks undergo chemical reactions, which break down the bonds holding the rocks together and cause rocks to fall apart. Oxidation, hydrolysis and carbonation are three most common types of chemical weathering. Generally, water is important for many chemical reactions and temperature can speed up these chemical reactions. Therefore, the average annual precipitation and temperature are two most important climatic factors that affect chemical weathering intensity. Recently, the chemical weathering intensity and element migration features of a loess profile in Eastern China has been studied (Chen et al. 2008). The results showing precipitation play a more important role than temperature in influencing the process of chemical weathering in warm and moist climate conditions. In this study area, Shilin, the average annual temperature is 16.3 °C, and the average annual precipitation is 800–850 mm. Moreover, the precipitation occurs from May to September, which accounts for more than 70% of the total annual precipitation, mostly in the form of showers and rainstorms. The scouring force exerted by rainfall coupled with chemical weathering can weaken and even breakdown the rocks. A thin, porous covering and new soil particles are formed during this process (Anderson et al. 2007). At the same time, the impact of raindrops on the soil surface can also break down soil aggregates and disperse the aggregate material. Moreover, in karst slope raindrops are prone to runoff due to the steep slopes, accordingly soil particles and organic matter are easily removed, which leads to soil erosion. Therefore, chemical weathering can accelerate physical erosion. After physical erosion, the fresh mineral surface can contact with the air and water, which will also accelerate chemical weathering. That is why the physical erosion and chemical weathering are positively correlated in this study.

Conclusions

In the eroded soil profiles, the ^{137}Cs are mainly distributed in the topsoil between 0 and 6 cm with a negative exponential. At the hillside, the maximum of ^{137}Cs appears in the topsoil, whereas at the hilltop, the maximum appears in the subsurface of the soil. Meanwhile, the specific activity of ^{137}Cs increases along the slope. Therefore, topography and slope are two factors that affect the rates of soil erosion. Also, a classical soil erosion model was used to estimate the soil erosion and sedimentation rates at different locations of the slope. The results show the soil erosion intensity decreases along the slope, and sedimentation locates at the bottom and the washland, indicating the formation of soil is a combination of hilltop erosion and bottom sedimentation in this area. The soil erosion intensity falls within the range from mild to moderate erosion. However, the nutrients in the surface soil will be lost with the erosion, and the soil material circulation may be in an unbalanced state. All these could bring direct harm to the local ecology, which shall draw a great attention. The distribution of TOC, TN and TP contents along the soil profiles are similar in this study. And the carbon and nitrogen storage capacity of 0–5 cm soil are better than that of 20–40 cm. Moreover, the ^{137}Cs distribution of all profiles is positively correlated with the TOC, TN and TP contents. This is because there is a large amount of soil nutrient loss in areas where soil erosion rates are high. As the soil erosion proceeds, the soil quality declines with potential damages to the ecological environment in the surrounding area. The chemical index of alteration and Na/K value both show that the soil in the study area is at the stage of strong chemical weathering under the subtropical conditions, and their changes along the slope are basically consistent with the changes of soil erosion rates. A–CN–K ternary diagram illustrates a similar weathering process among five profiles, that is, the early leaching of Ca, Na, K and later enrichment of Al and Fe. In addition, the study on the relationship between soil erosion rates, chemical weathering intensity and nutrient elements is preliminary, and it is necessary to do more research on the correlation between the slope length, the soil geochemical characteristics and soil erosion rates in the future. The soil erosion model, which establishes the relationship between soil erosion rates and the distribution characteristics of ^{137}Cs along the soil profile, also needs to be improved to better estimate the soil erosion rates and obtain its pattern of spatial differentiation.

Acknowledgements The authors gratefully acknowledge the anonymous reviewers for their constructive comments and suggestions, which undoubtedly have helped in improving this research paper. This work was jointly supported from the National Natural Science Foundation of China (no. 41473122), the National Key Basic Research and Development Program (no. 2013CB956702) and the Hundred Talents Programs of Chinese Academy of Sciences.

References

Anderson SP, Blanckenburg FV, White AF (2007) Physical and chemical controls on the critical zone. Elements 3(5):315–319. https://doi.org/10.2113/gselements.3.5.315

Babechuk MG, Widdowson M, Kamber BS (2014) Quantifying chemical weathering intensity and trace element release from two contrasting basalt profiles, Deccan Traps, India. Chem Geol 363:56–75. https://doi.org/10.1016/j.chemgeo.2013.10.027

Bai X (2011) Assessment of sediment and erosion rates by using the caesium-137 technique in a Chinese polygonal karst depression. Environ Earth Sci 64(8):2151–2158. https://doi.org/10.1007/s1265-011-1042-8

Bathrellos GD, Gaki-Papanastassiou K, Skilodimou HD, Papanastassiou D, Chousianitis KG (2012) Potential suitability for urban planning and industry development using natural hazard maps and geological–geomorphological parameters. Environ Earth Sci 66(2):537–548. https://doi.org/10.1007/s12665-011-1263-x

Bathrellos GD, Skilodimou HD, Chousianitis K, Youssef AM, Pradhan B (2017) Suitability estimation for urban development using multi-hazard assessment map. Sci Total Environ 575:119–134. https://doi.org/10.1016/j.scitotenv.2016.10.025

Bian HY, Pang JL, Huang C, Zha XC, Gao PK, Wang XJ, Li X, Wang LB (2014) A comparative study of chemical weathering intensity and element transport features of loess-palaeosol in the upper reaches of Hanjiang and Weihe river valleys, China. Geogr Res 33(4):654–664. https://doi.org/10.11821/dlyj201404006

Blanckenburg FV (2005) The control mechanisms of erosion and weathering at basin scale from cosmogenic nuclides in river sediment. Earth Planert Sc Lett 242(3–4):224–239. https://doi.org/10.1016/j.epsl.2005.11.017

Braun JJ, Ngoupayou JRN, Viers J, Dupre B, Bedimo JPB, Boeglin JL, Robain H, Nyeck B, Freydier R, Nkamdjou LS, Rouiller J, Muller JP (2005) Present weathering rates in a humid tropical watershed: Nsimi, South Cameroon. Geochim Cosmochim Acta 69(2):357–387. https://doi.org/10.1016/j.gca.2004.06.022

Buttafuoco G, Conforti M, Aucelli PPC, Robustelli G, Scarciglia F (2012) Assessing spatial uncertainty in mapping soil erodibility factor using geostatistical stochastic simulation. Environ Earth Sci 66(4):1111–1125. https://doi.org/10.1007/s12665-01101317-0

Chen YY, Li XS, Han ZY, Yang SY, Yang SY, Wang YB, Yang DY (2008) Chemical weathering intensity and element migration features of the Xiashu loess profile in Zhenjiang, Jiangsu Province. J Georg Sci 18(3):341. https://doi.org/10.1007/s11442-008-0341-9

Chetelat B, Liu CQ, Zhao ZQ, Wang QL, Li SL, Li J, Wang BL (2008) Geochemistry of the dissolved load of the Changjiang Basin rivers: anthropogenic impacts and chemical weathering. Geochim Cosmochim Acta 72(17):4254–4277. https://doi.org/10.1016/j.gca.2008.06.013

Clift PD, Wan S, Blusztajn J (2014) Reconstructing chemical weathering, physical erosion and monsoon intensity since 25 Ma in the northern South China Sea: A review of competing proxies. Earth-Sci Rev 130:86–102. https://doi.org/10.1016/j.earscirev.2014.01.002

Dai Q, Liu Z, Shao H, Yang Z (2015) Karst bare slope soil erosion and soil quality: a simulation case study. Solid Earth 6(3):985–995. https://doi.org/10.5194/se-6-985-2015

Feng T, Chen HS, Polyakov VO, Wang KL, Zhang XB, Zhang W (2016) Soil erosion rates in two karst peak-cluster depression basins of northwest Guangxi, China: comparison of the RUSLE model with ^{137}Cs measurements. Geomorphology 253:217–224. https://doi.org/10.1016/j.geomorph.2015.10.013

Ferrier KL, Kirchner JW (2008) Effects of physical erosion on chemical denudation rates: a numerical modeling study of soil-mantled hillslopes. Earth Plan Sci Lett 272(3–4):591–599. https://doi.org/10.1016/j.epsl.2008.05.024

Fu X, Shao M, Wei X, Horton R (2010) Soil organic carbon and total nitrogen as affected by vegetation types in Northern Loess Plateau of China. Geoderma 155(1–2):31–35. https://doi.org/10.1016/j.geoderma.2009.11.020

Gabet EJ (2007) A theoretical model coupling chemical weathering and physical erosion in landslide-dominated landscapes. Earth Planert Sc Lett 264(1–2):259–265. https://doi.org/10.1016/j.epsl.2007.09.028

Gabet EJ, Mudd SM (2009) A theoretical model coupling chemical weathering rates with denudation rates. Geology 37(2):151–154. https://doi.org/10.1130/G25270A.1

Gaspar L, Navas A, Walling DE, Machin J, Arozamena JG (2013) Using ^{137}Cs and $^{210}Pb_{ex}$ to assess soil redistribution on slopes at different temporal scales. Catena 102:46–54. https://doi.org/10.1016/j.catena.2011.01.004

Gelaw AM, Singh BR, Lal R (2014) Soil organic carbon and total nitrogen stocks under different land uses in a semi-arid watershed in Tigray, Northern Ethiopia. Agric Ecosys Environ 188:256–263. https://doi.org/10.1016/j.agee.2014.02.035

Henry A, Mabit L, Jaramillo RE, Cartagena Y, Lynch JP (2013) Land use effects on erosion and carbon storage of the Río Chimbo watershed, Ecuador. Plant Soil 367(1–2):477–491. https://doi.org/10.1007/s11104-012-1478-y

Kautz CQ, Martin CE (2007) Chemical and physical weathering in New Zealand's Southern Alps monitored by bedload sediment major element composition. Appl Geochem 22(8):1715–1735. https://doi.org/10.1016/j.apgeochem.2007.03.031

Kavian A, Azmoodeh A, Solaimani K (2014) Deforestation effects on soil properties, runoff and erosion in northern Iran. Arab J Geosci 7(5):1941–1950. https://doi.org/10.1007/s12517-013-0853-1

Kheir RB, Abdallah C, Khawlie M (2008) Assessing soil erosion in Mediterranean karst landscapes of Lebanon using remote sensing and GIS. Eng Geol 99(3–4):239–254. https://doi.org/10.1016/j.enggeo.2007.11.012

Kirchner JW, Riebe CS, Ferrier KL, Finkel RC (2006) Cosmogenic nuclide methods for measuring long-term rates of physical erosion and chemical weathering. J Geochem Explor 88(1–3):296–299. https://doi.org/10.1016/j.gexplo.2005.08.060

Krishnaswamo S, Gyana RT (2012) Chemical and physical erosion of river Basins of India: links to climate. Proc Indian Nat Sci Acad 78(3):299–311

Kurtz AC, Derry LA, Chadwick OA (2001) Accretion of Asian dust to Hawaiian soils: isotopic, elemental, and mineral mass balances. Geochim Cosmochim Acta 65(12):1971–1983. https://doi.org/10.1016/S0016-7037(01)00575-0

Lanznaster M, Hratchian HP, Heeg MJ, Hryhorcauk LM, Mcgarvey BR, Schleqel HB, Verani CN (2010) Relating soil erosion and sediment yield to geomorphic features and erosion processes at the catchment scale in the Spanish pre-pyrenees. Environ Earth Sci 61(1):143–158. https://doi.org/10.1007/s12665-009-0332-x

Lenka NK, Dass A, Sudhishri S, Patnaik US (2012) Soil carbon sequestration and erosion control potential of hedgerows and grass filter strips in sloping agricultural lands of eastern India. Agric Ecosyst Environ 158:31–40. https://doi.org/10.1016/j.agee.2012.05.017

Li M, Li Z, Yao W, Liu P (2009) Estimating the erosion and deposition rates in a small watershed by the ^{137}Cs tracing method. Appl Radiat Isotopes 67(2):362–366. https://doi.org/10.1016/j.apradiso.2008.10.011

Li Y, Bai XY, Zhou YC, Luo YQ, Tian X, Tian YC, Li PL (2016) Spatial–temporal evolution of soil erosion in a typical mountainous Karst Basin in SW China, based on GIS and RUSLE. Arab J Sci Eng 41(1):209–221. https://doi.org/10.1007/s13369-015-1742-6

Mclennan SM (1993) Weathering and Global Denudation. J Geol 101(2):295–303. https://doi.org/10.1086/648222

Millot R, Gaillardet J, Dupré B, Allègr CJ (2002) The global control of silicate weathering rates and the coupling with physical erosion: new insights from rivers of the Canadian Shield. Earth Plan Sci Lett 196(1–2):83–98. https://doi.org/10.1016/S0012-821X(01)00599-4

Mitchell AK, Barclay HJ, Brix H, Pollard DFW, Benton R, Dejong R (1996) Biomass and nutrient element dynamics in Douglas-fir: effects of thinn. Can J Forest Res 26(3):376–388. https://doi.org/10.1139/x26-042

Molla T, Sisheber B (2017) Estimating soil erosion risk and evaluating erosion control measures for soil conservation planning at Koga watershed in the highlands of Ethiopian. Solid Earth 8(1):13. https://doi.org/10.5194/se-8-13-2017

Nesbitt HW, Young GM (1982) Early Proterozoic climates and plate motions inferred from major element chemistry of lutites. Nature 299(5885):715–717. https://doi.org/10.1038/299715a0

Nesbitt HW, Young GM (1989) Formation and diagenesis of weathering profiles. J Geol 97(2):129–147. https://doi.org/10.1086/629290

Nesbitt HW, Young GM, Mclennan SM, Keays RR (1996) Effects of chemical weathering and sorting on the petrogenesis of siliciclastic sediments, with implications for provenance studies. J Geol 104(5):525–542. https://doi.org/10.1086/629850

Niu XY, Wang YH, Yang H, Zhang JW, Wu SS, Xie B (2014) Effects of different land uses on soil erosion and soil nutrient variability in the shuanglong catchment of dianchi watershed. Res Environ Sci 27:1043–1050. https://doi.org/10.1016/s1002-0160(14)60080-1 (in chinese).

Nosrati K, Haddadchi A, Zare MR, Shirzadi L (2015) An evaluation of the role of hillslope components and land use in soil erosion using Cs-137 inventory and soil organic carbon stock. Geoderma 243:29–40. https://doi.org/10.1016/j.geoderma.2014.12.008

Papadopoulou-Vrynioti K, Bathrellos GD, Skilodimou HD, Kaviris G, Makropoulos K (2013) Karst collapse susceptibility mapping considering peak ground acceleration in a rapidly growing urban area. Eng Geol 158:77–88. https://doi.org/10.1016/j.enggeo.2013.02.009

Parise M, Closson D, Gutiérrez F, Stevanović Z (2015) Anticipating and managing engineering problems in the complex karst environment. Environ Earth Sci 74(12):7823–7835. https://doi.org/10.1007/s12665-015-4647-5

Peng T, Wang SJ (2012) Effects of land use, land cover and rainfall regimes on the surface runoff and soil loss on karst slopes in southwest China. Catena 90:53–62. https://doi.org/10.1016/j.catena.2011.11.001

Perović V, Životić L, Kadović R, Đorđević A, Jaramaz D, Mrvić V, Todorović M (2013) Spatial modelling of soil erosion potential in a mountainous watershed of South-eastern Serbia. Environ Earth Sci 68(1):115–128. https://doi.org/10.1007/s12665-012-1720-1

Pumpanen J, Ohashi M, Endo I, Hari P, Back J, Kulmala M, Ohte N (2016) ^{137}Cs distributions in soil and trees in forest ecosystems after the radioactive fallout—comparison study between southern Finland and Fukushima, Japan. J Environ Radioact 161:73–81. https://doi.org/10.1016/j.jenvrad.2016.04.024

Ritchie JC, McCarty GW, Venteris ER, Kaspar TC (2007) Soil and soil organic carbon redistribution on the landscape. Geomorphology 89(1–2):163–171. https://doi.org/10.1016/j.geomorph.2006.07.021

Rozos D, Skilodimou HD, Loupasakis C, Bathrellos GD (2013) Application of the revised universal soil loss equation model on landslide prevention. An example from N. Euboea (Evia) Island, Greece. Environ Earth Sci 70(7):3255–3266. https://doi.org/10.1007/s12665-013-2390-3

Schoonejans J, Vanacker V, Opfergelt S, Ameijeiras-Mariño Y, Christl M (2016) Kinetically limited weathering at low denudation rates in semiarid climatic conditions. J Geophys Res-Earth 121(2):336–350. https://doi.org/10.1002/2015JF003626

Shao JQ, Yang SY, Li C (2012) Chemical indices (CIA and WIP) as proxies for integrated chemical weathering in China: inferences from analysis of fluvial sediments. Sediment Geol 265:110–120. https://doi.org/10.1016/j.sedgeo.2012.03.020

Takahashi J, Tamura K, Suda T, Marsumura R, Onda Y (2015) Vertical distribution and temporal changes of ^{137}Cs in soil profiles under various land uses after the Fukushima Dai-ichi Nuclear Power Plant accident. J Environ Radioact 139:351–361. https://doi.org/10.1016/j.jenvrad.2014.07.004

Tang CQ, Li YH, Zhang ZY (2010) Species diversity patterns in natural secondary plant communities and man-made forests in a subtropical mountainous karst area, Yunnan, SW China. Mt Res Dev 30(3):244–251. https://doi.org/10.1659/MRD-JOURNAL-D-10-00021.1

Tripathi R, Nayak AK, Bhattacharyya P, Shukla AK, Shahid M, Raja R, Panda R, Panda BB, Mohanty S, Kumar A (2014) Soil aggregation and distribution of carbon and nitrogen in different fractions after 41 years long-term fertilizer experiment in tropical rice–rice system. Geoderma 213:280–286. https://doi.org/10.1016/j.geoderma.2013.08.031

Verheijen FGA, Jones RJA, Rickson RJ, Smith CJ (2009) Tolerable versus actual soil erosion rates in Europe. Earth-Sci Rev 94(1–4):23–38. https://doi.org/10.1016/j.earscirev.2009.02.003

Walling DE, Owens PN (1996) Spatial variability of caesium-137 inventories at reference sites: an example from two contrasting sites in England and Zimbabwe. Appl Radiat Isotopes 47(7):699–707. https://doi.org/10.1016/0969-8043(96)00015-2

Wang JX, Zou BP, Liu Y, Tang YQ, Zhang XB, Yang P (2014) Erosion-creep-collapse mechanism of underground soil loss for the karst rocky desertification in Chenqi village, Puding county, Guizhou, China. Environ Earth Sci 72(8):2751–2764. https://doi.org/10.1007/s1665-014-3182-0

Xu ZF, Liu CQ (2007) Chemical weathering in the upper reaches of Xijiang River draining the Yunnan–Guizhou Plateau, Southwest China. Chem Geol 239(1–2):83–95. https://doi.org/10.1016/j.chemgeo.2006.12.008

Yang JS, Liu JS, Hu XJ, Li XX, Wang Y, Li HY (2013) Changes of soil organic carbon, nitrogen and phosphorus concentrations under different land uses in marshes of Sanjiang Plain. Acta Ecol Sin 33(6):332–337. https://doi.org/10.1016/j.chnaes.2013.09.007

Yang Q, Xie Y, Li W, Jiang ZC, Li H, Qin XM (2014) Assessing soil erosion risk in karst area using fuzzy modeling and method of the analytical hierarchy process. Environ Earth Sci 71(1):287–292. https://doi.org/10.1007/s12665-013-2432-x

Zhang XB, Higgitt DL, Walling DE (1990) A preliminary assessment of the potential for using caesium-137 to estimate rates of soil erosion in the Loess Plateau of China. Hydrol Sci J 35(3):243–252. https://doi.org/10.1080/02626669009492427

Zhang X, He Z, Xue D (2010) Analysis on water and soil erosion of dongchuan area in Jinsha Valley. J Catastrophol 25(1):50–53. https://doi.org/10.3969/j.issn.1000-811X.2010.01.011 (in chinese).

Zhang C, Liu G, Xue S, Sun C (2013) Soil organic carbon and total nitrogen storage as affected by land use in a small watershed of the Loess Plateau, China. Eur J Soil Biol 54:16–24. https://doi.org/10.1016/j.ejsobi.2012.10.007